

Cite this article as: Li Xuejun, Liu Ying, Ye Jinwen, et al. Effect of Carbon Content on Microstructure and Wear Resistance of Fe-Cr-C/TiCN Composites by Spark Plasma Sintering[J]. Rare Metal Materials and Engineering, 2021, 50(07): 2273-2280.

ARTICLE

# Effect of Carbon Content on Microstructure and Wear Resistance of Fe-Cr-C/TiCN Composites by Spark Plasma Sintering

Li Xuejun, Liu Ying, Ye Jinwen, Zhou Tingchuan, Chen Daoying

College of Materials Science and Engineering, Sichuan University, Chengdu 610065, China

**Abstract:** Fe-Cr-C/TiCN composites with different carbon contents were prepared via mechanical alloying followed by spark plasma sintering. The effects of carbon black content on the microstructure and wear properties of Fe-Cr-C/TiCN composites were systematically investigated by scanning electron microscopy, X-ray diffraction, Vickers hardness test, and ball-on-disk type tribotest. The results show that the  $(\text{Cr, Fe})_7\text{C}_3$  carbides form in the sintered specimens with 1wt%~5wt% carbon, but  $(\text{Cr, Fe})_3\text{C}$  phases appear when the carbon black content reaches 4wt%~5wt%. Carbon black content plays a significant role in the microstructure uniformity and densification of the Fe-Cr-C/TiCN composites. When the sintering temperature is  $\sim 1000$  °C, the relative density of specimen without carbon addition increases from 95.0% to 99.7% of the specimen with carbon addition of 3wt%, indicating that the full densification is realized. High Vickers hardness of 11 940 MPa is achieved for the specimen with carbon addition of 3wt%. Furthermore, adding an appropriate amount of carbon (3wt%) contributes to the excellent wear properties with narrow fluctuation ranges of friction coefficient, suggesting an average friction coefficient of 0.320 and wear rate of  $6.8 \times 10^{-4} \text{ mm}^3 \cdot \text{N}^{-1} \cdot \text{m}^{-1}$ .

**Key words:** Fe-Cr-C/TiCN composites; carbon; spark plasma sintering; microstructure and wear resistance

TiCN-reinforced iron-based composite materials have attracted much attention due to their high hardness, excellent wear resistance, good thermal stability, low cost, and enhanced properties by heat treatment<sup>[1-4]</sup>. Liquid phase sintered Fe/TiCN composites have the weaknesses of poor sintering activity, which generally causes embrittlement. This disadvantage has been improved by adding alloying elements, such as Cr<sup>[5]</sup>, Mo<sup>[6]</sup>, W<sup>[7]</sup>, and Ni<sup>[8]</sup>, or optimizing the fabrication process, including the in-situ synthesis<sup>[9]</sup> and powder metallurgy routes. For example, high-speed steel<sup>[10,11]</sup> and Cr-Mo low-alloy steel<sup>[1]</sup> are often used as the matrix of Fe/TiCN composites because of the components of Cr, Mo, and other elements. Meanwhile, the 430L stainless steel is also selected as the matrix of Fe/TiCN composites, and additional carbon can optimize the microstructure and hardness of the composites<sup>[12]</sup>. It seems that iron-based alloys are good candidates for the matrix phases of Fe/TiCN composites to obtain desirable sintering activities and physical performances. Among these

alloys, the high chromium cast iron with  $M_7C_3$  ( $M$ : Fe and Cr) carbide forming at a certain Cr/C ratio<sup>[13]</sup> is promising to prepare Fe/TiCN composites, due to its excellent hardness and wear resistance. However, few studies reported about it.

It is well known that the content of carbon and chromium plays an essential role in the formation and morphology of  $M_7C_3$  carbides.  $M_7C_3$  carbides are reported to be synthesized by mechanical alloying of amorphous carbon and chromium powders and sintering at  $\sim 1400$  °C<sup>[14]</sup>.  $M_7C_3$  carbides form in the shape of square bars and are uniformly distributed in the matrix by super solid-liquid phase sintering with gas atomized high-chromium cast iron powders (19.6wt% Cr, 2.7wt% C) as raw materials<sup>[15]</sup>. To date, most of the high-chromium cast iron-based composites were fabricated by traditional powder metallurgy<sup>[16]</sup> and cast process<sup>[17-20]</sup>. However, because of the rapid grain growth caused by the formation of iron-based liquid phase, such methods require high sintering temperatures and usually lead to coarse microstructures. Conse-

Received date: July 15, 2020

Foundation item: National Key Research and Development Plan of China (2017YFB0305900); Sichuan Science and Technology Program (2020ZDZX0008)

Corresponding author: Liu Ying, Ph. D., Professor, College of Materials Science and Engineering, Sichuan University, Chengdu 610065, P. R. China, Tel: 0086-28-85405332, E-mail: liuying5536@scu.edu.cn

Copyright © 2021, Northwest Institute for Nonferrous Metal Research. Published by Science Press. All rights reserved.

quently, the sintering temperatures of Fe-Cr-C/TiCN composites need to reduce to simultaneously control the grain sizes and high densification.

The spark plasma sintering (SPS) have the advantages of lower sintering temperatures, shorter sintering time, and faster heating rate<sup>[21-23]</sup>, and the high wear resistance of  $M_7C_3$  carbides can be retained with the appropriate carbon black content in the composites. Based on the above considerations, the introduction of  $M_7C_3$  carbides into Fe-Cr-C/TiCN composites and the application of SPS technique were chosen to simultaneously achieve the uniform and dense microstructure with high hardness and wear resistance. In this research, the carbon black content of composites was changed to systematically study its effect on the microstructure, phase evolutions, Vickers hardness, and wear resistance of Fe-Cr-C/TiCN composites.

## 1 Experiment

Carbonyl iron powders ( $D_{50} \approx 1.4 \mu\text{m}$ ), chromium powders ( $D_{50} \approx 10.9 \mu\text{m}$ ), titanium carbonitride powders ( $D_{50} \approx 5.2 \mu\text{m}$ ), and carbon black powders ( $D_{50} \approx 0.9 \mu\text{m}$ ) were used as raw materials, and their morphologies were obtained by a scanning electron microscopy (SEM, JSM-6490LV, Japan), as shown in Fig. 1. The composition of Fe-Cr-xC/TiCN ( $x=0\sim 5$ ) composites is listed in Table 1. Powders of carbonyl iron, chromium, titanium carbonitride, and carbon black were mixed in the QM-1SP4 planetary ball mill using alcohol as medium under argon atmosphere at a speed of 400 r/min for 12 h, and argon acted as a protective atmosphere to prevent the powders from oxidation during milling. Tungsten carbide balls with different sizes (6, 10, and 15 mm) were used in the ball mill, and the mass ratio of balls to powders was 7:1. Afterward, the mixed slurry was dried in a vacuum oven at 60 °C for 6 h. In order to

improve the fluidity and sphericity of powders, the granulation process was used. Finally, the powders were passed through a 150# mesh sieve. The powders were poured into a graphite mold with the diameter of 20 mm, where carbon paper was used to facilitate demolding. The powders were sintered in a vacuum SPS system (SPS-1050, Sumitomo, Japan) under a pressure of 30 MPa at 1000 °C for 10 min. After the specimen was taken out of the mold, the carbon paper was removed using sandpapers of 180#, 240#, 400#, 800#, 1000#, and 1500# sequentially in a grinding machine, followed by a diamond polishing for 10 min.

The particle size of raw powders was measured by a laser particle size analyzer (HELOS-RODOS/M, Germany). The phase structures were analyzed by X-ray diffraction (XRD, DX-2700, China) using Cu K $\alpha$  radiation at a scanning rate of 0.06°/s in the range of  $2\theta=30^\circ\sim 90^\circ$ . The microstructures of the raw materials and sintered specimens were observed by SEM equipped with an energy dispersive spectroscopy (EDS). The density of sintered specimen was measured by the Archimedes method. The specimen density is calculated according to Eq.(1):

$$\rho = \frac{\rho_1 m_1}{m_2} \quad (1)$$

where  $m_1$  is the mass of specimen weighed in air,  $\rho_1$  is the density of distilled water, and  $m_2$  is the mass of specimen weighed in water.

The theoretical density is expressed by Eq.(2) as follows:

$$\rho_t = \frac{1}{\sum \frac{m_i}{\rho_i}} \quad (2)$$

where  $m_i$  and  $\rho_i$  with  $i=\text{Fe, Cr, C, TiCN}$  are the mass fraction and theoretical density of Fe, Cr, C, and TiCN, respectively.

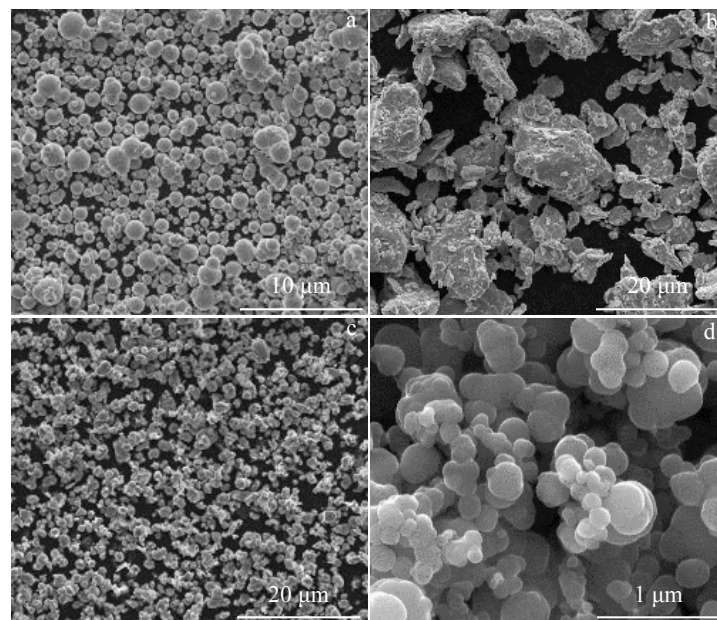


Fig.1 SEM morphologies of raw material powders of Fe (a), Cr (b),  $\text{TiC}_{0.7}\text{N}_{0.3}$  (c), and carbon black (d)

**Table 1** Composition of Fe-Cr-xC/TiCN composites (wt%)

| x | Cr | C | TiC <sub>0.7</sub> N <sub>0.3</sub> | Fe   |
|---|----|---|-------------------------------------|------|
| 0 | 15 | 0 | 15                                  | Bal. |
| 1 | 15 | 1 | 15                                  | Bal. |
| 2 | 15 | 2 | 15                                  | Bal. |
| 3 | 15 | 3 | 15                                  | Bal. |
| 4 | 15 | 4 | 15                                  | Bal. |
| 5 | 15 | 5 | 15                                  | Bal. |

Finally, the relative density can be obtained by Eq. (3) as follows:

$$\rho_r = \frac{\rho}{\rho_t} \quad (3)$$

In this study, the density of each specimen was tested three times, and the average value was taken as the density of the specimen.

The hardness was measured at least five times using 452SVA Wolpert Wilson Instruments at a load of 49 N with a dwelling time of 15 s. The wear resistance was tested by a ball-on-disk type tribometer (HT-1000, China) under a load of 9.8 N at 1000 r/min for 40 min. In this measurement, Si<sub>3</sub>N<sub>4</sub> ceramic balls with a diameter of 6 mm were selected as the counter-material, and the friction coefficient was continuously recorded by software. The wear rate was calculated by Eq.(4) as follows<sup>[24]</sup>:

$$\omega = \frac{\Delta m}{\rho FL} \quad (4)$$

where  $\omega$  is the wear rate,  $\Delta m$  is the mass loss,  $\rho$  is the density,  $F$  is the applied loading force, and  $L$  is the sliding distance.

## 2 Results and Discussion

### 2.1 Phase components and microstructure

Fig.2 presents the XRD patterns of the SPS sintered Fe-Cr-xC/TiCN ( $x=0\sim5$ ) composites.  $\alpha$ -Fe phase and TiC<sub>0.7</sub>N<sub>0.3</sub> phase can be observed in the specimen without carbon addition. The (Cr, Fe)<sub>7</sub>C<sub>3</sub> phase appears in Fe-Cr-xC/TiCN composites with

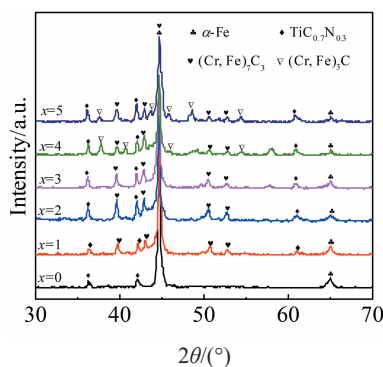


Fig.2 XRD patterns of SPS sintered Fe-Cr-xC/TiCN ( $x=0\sim5$ ) composites

$x=1\sim3$ . The (Cr, Fe)<sub>3</sub>C and (Cr, Fe)<sub>7</sub>C<sub>3</sub> phases form simultaneously in Fe-Cr-xC/TiCN composites with  $x=4, 5$ . According to the phase diagram of Fe-Cr-C systems<sup>[25]</sup>,  $M_{23}C_6$  ( $M=Fe, Cr$ ),  $M_7C_3$  ( $M=Fe, Cr$ ), and  $M_3C$  ( $M=Fe, Cr$ ) carbides form in sequence with the decrease of the Cr/C ratio when the chromium content ranges from 13wt% to 17wt% in the Fe-Cr-C systems. In this study, no  $M_{23}C_6$  carbide is detected in Fe-Cr-xC/TiCN ( $x=0\sim5$ ) composites, but  $M_7C_3$  and  $M_3C$  can be observed, which may be due to the weak atomic diffusion during solid-phase sintering.

Fig. 3 shows the backscattered electron (BSE) images of SPS sintered Fe-Cr-xC/TiCN ( $x=0\sim5$ ) composites. Most of TiCN particles are nearly spherical, suggesting that there is no major reaction between the TiCN particles and the matrix because of the excellent thermal stability of TiCN and the absence of the liquid phase during sintering. Without the addition of carbon black, spherical TiCN particles are embedded in matrix, but there are coarse chromium-rich phases. After the addition of carbon black in Fe-Cr-xC/TiCN ( $x=1\sim4$ ) composites, the coexisted black phase, gray phase, and gray-black phase become differentiated, referring to TiCN, matrix, and Fe-Cr carbides, respectively, based on the EDS analysis results in Table 2. The EDS results show that the ratio of  $M$  (Fe+Cr) to C is close to 7:3 in the Fe-Cr carbide (gray-black) phase, suggesting that it is (Cr, Fe)<sub>7</sub>C<sub>3</sub>, as further identified by XRD analysis. White phase state is observed in Fe-Cr-xC/TiCN composite with  $x=5$ , and the phase contains iron with a small amount of chromium and carbon based on EDS results (Table 2), which roughly refers to the ferrite phase. The formation of carbides consumes chromium and carbon, and the remaining chromium dissolves into iron to form Fe-Cr solid solution, resulting in the formation of ferrites from the remained iron. Therefore, it can be concluded that the content of carbon has a significant effect on the microstructures of composites, and adding an appropriate amount of carbon black (3wt%) is conducive to achieving the uniform microstructure.

### 2.2 Relative density and Vickers hardness

The relative density and Vickers hardness of SPS sintered Fe-Cr-xC/TiCN ( $x=0\sim5$ ) composites are exhibited in Fig.4. To estimate the relative density of the Fe-Cr-xC/TiCN composites, the theoretical density of the composites is calculated using the theoretical densities of Fe (7.87 g/cm<sup>3</sup>), Cr (7.19 g/cm<sup>3</sup>), C (1.80 g/cm<sup>3</sup>), and TiC<sub>0.7</sub>N<sub>0.3</sub> (5.18 g/cm<sup>3</sup>). Obviously, the relative density and Vickers hardness show a similar tendency with the change of carbon black content, which increases rapidly with the increase of carbon black content ( $x=0\sim3$ ), and then increases slowly. The Fe-Cr-xC/TiCN composite with  $x=0$  displays a lower relative density (95.0%) and hardness, because the amount of hard carbides is much smaller. As the carbon black content increases from 1wt% to 3wt%, the relative density and hardness increase from 96.4% and 9740 MPa to 99.7% and 11 940 MPa, respectively. The SEM images of specimens ( $x=0\sim3$ ) for porosity measurement is shown in Fig.5, indicating that the porosity decreases with the increase of carbon black content. Such a high relative

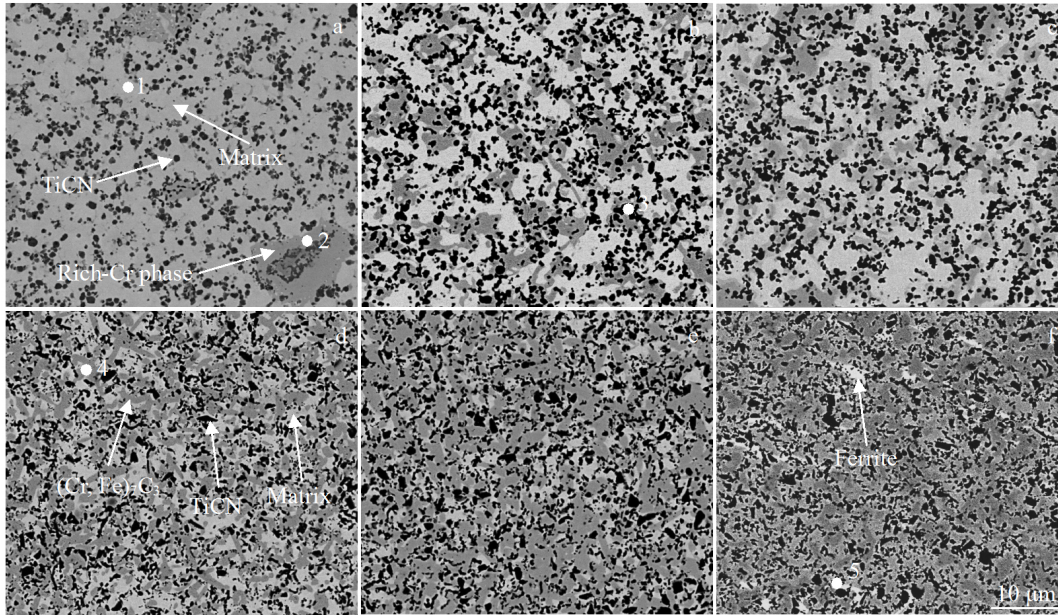


Fig.3 SEM-BSE images of Fe-Cr-xC/TiCN composites: (a)  $x=0$ , (b)  $x=1$ , (c)  $x=2$ , (d)  $x=3$ , (e)  $x=4$ , and (f)  $x=5$

Table 2 EDS results of the points in Fig.3 (at%)

| Point | Phase    | Fe   | Cr   | C    | N    | Ti   |
|-------|----------|------|------|------|------|------|
| 1     | Matrix   | 77.8 | 19.8 | 2.4  | -    | -    |
| 2     | Rich-Cr  | 20.7 | 61.9 | 17.4 | -    | -    |
| 3     | TiCN     | -    | -    | 33.6 | 14.0 | 52.4 |
| 4     | $M_7C_3$ | 44.5 | 26.7 | 28.8 | -    | -    |
| 5     | Ferrite  | 84.7 | 5.8  | 9.5  | -    | -    |

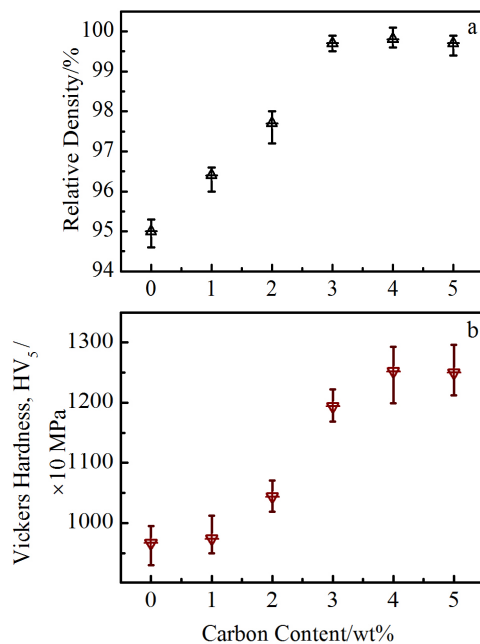


Fig.4 Relative density (a) and Vickers hardness (b) of SPS sintered Fe-Cr-xC/TiCN ( $x=0\sim 5$ ) composites

density is related to the fact that carbon black reduces the liquidus temperature of Fe-Cr-C/TiCN composites to promote densification during sintering, as suggested by other researchers<sup>[26]</sup>. The increase in hardness is mainly due to the large amount of uniformly distributed carbides (Fig. 3d) and the highly increased relative density. When the carbon black content further increases ( $x \geq 4$ ), the relative density is almost unchanged as it approaches to the theoretical density. Nevertheless, the hardness increases to  $\sim 12\ 500$  MPa for Fe-Cr-xC/TiCN composites with  $x=4, 5$  due to more uneven carbides.

### 2.3 Wear resistance

The evolution of the friction coefficient for the SPS sintered Fe-Cr-xC/TiCN ( $x=0\sim 5$ ) composites is shown in Fig. 6. Apart from the severe wear stage (the wear time is not long enough), two typical stages are identified, including the running-in stage and the stable wear stage. The fluctuation range of friction coefficient in the stable wear stage is marked with the red dots. When  $x=0$ , the friction coefficient rapidly increases to the maximum value of 0.366 during the running-in stage of about 200 s. During the stable wear stage, the friction coefficient fluctuates within the ranges of about 0.082 with the mean friction coefficient of 0.280. For the Fe-Cr-xC/TiCN composite with  $x=1$ , the duration of its running-in stage ( $\sim 150$  s) is shorter than that of composite without carbon black addition, but the fluctuation range in the stable wear stage significantly increases to  $\sim 0.132$ , as shown in Fig. 6b. When  $x=2$  and 3, the specimens show a shorter running-in stage ( $\sim 60$  s) and higher average friction coefficients (0.340 and 0.320). However, the fluctuation range of Fe-Cr-xC/TiCN composite with  $x=2$  ( $\sim 0.111$ ) during the stable wear stage is larger than that of composite with  $x=3$  (0.084), which indicates that the

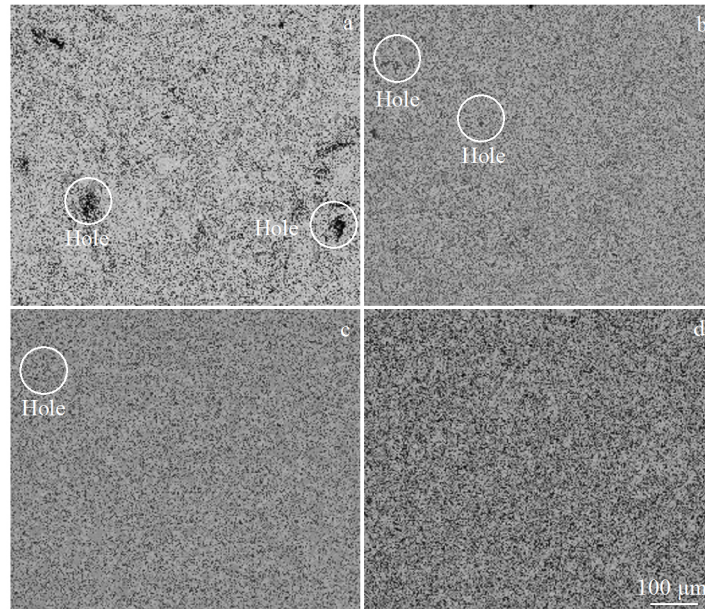


Fig.5 SEM images of Fe-Cr-xC/TiCN composites: (a)  $x=0$ , (b)  $x=1$ , (c)  $x=2$ , and (d)  $x=3$

running-in stage shortens. In contrast, the stability of the friction coefficient improves with the increase of the carbon black content, and the optimal carbon black content is 3wt%, which is related to the increase of volume fraction of  $(\text{Cr, Fe})_7\text{C}_3$ . For the Fe-Cr-xC/TiCN composites with  $x=4, 5$ , the friction coefficients and the fluctuation ranges ( $\sim 0.110$ ) increase significantly due to the uneven distribution of coarse  $(\text{Cr, Fe})_7\text{C}_3$  phase. Moreover, when  $x=5$ , the presence of soft ferrite causes the extension of the running-in stage to 200 s.

Fig. 7 exhibits the average friction coefficient (calculated

from the friction coefficient at 200 s during the stable wear stage) and wear rate of Fe-Cr-xC/TiCN composites ( $x=0\sim 5$ ). Similar to the behavior of Vickers hardness, the average friction coefficient basically shows an increasing tendency, resulting from the increase of hard carbides in number<sup>[27]</sup>. In terms of the wear rate, it dramatically decreases after adding carbon black, reaching the minimum value ( $\sim 6.8 \times 10^{-4} \text{ mm}^3 \cdot \text{N}^{-1} \cdot \text{m}^{-1}$ ) when  $x=3$ , and then increases with the increase of carbon black content. The decrease in the wear rate may be ascribed to the significant increase in hardness, while the subsequent increase

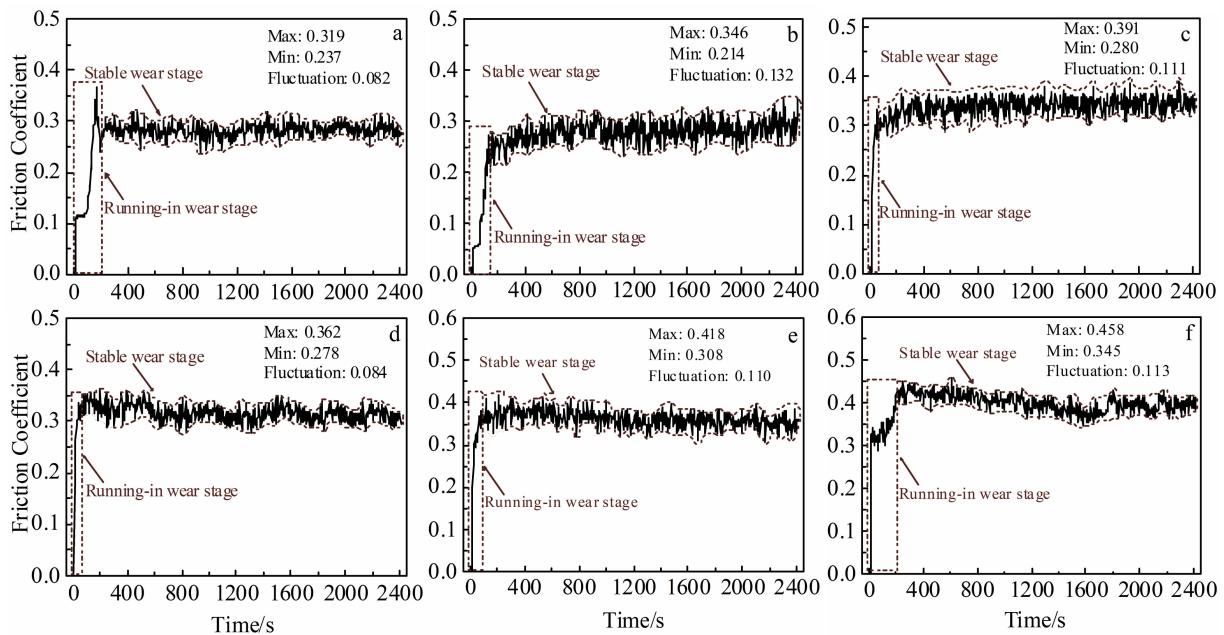


Fig.6 Evolution of friction coefficient for SPS sintered Fe-Cr-xC/TiCN composites: (a)  $x=0$ , (b)  $x=1$ , (c)  $x=2$ , (d)  $x=3$ , (e)  $x=4$ , and (f)  $x=5$

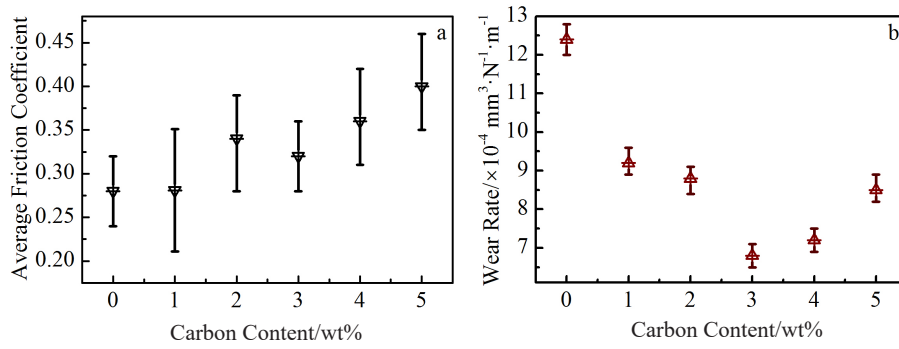


Fig.7 Average friction coefficient (a) and wear rate (b) of SPS sintered Fe-Cr-xC/TiCN ( $x=0\sim 5$ ) composites

is possibly caused by the uneven distribution of carbides.

To further study the surface evolution of the composites with different carbon black contents, the wear surface morphologies of the specimens with  $x=0\sim 4$  are shown in Fig.8. Obviously, the width of the wear track increases slightly with the increase of carbon black contents, because the volume loss of the  $\text{Si}_3\text{N}_4$  ball increases with the increase of composite hardness. When  $x=0$ , more spalling pits are clearly identified, and TiCN particles are evenly distributed in the Fe-Cr matrix (Fig.8a<sub>1</sub> and 8a<sub>2</sub>). Compared with the specimen with  $x=0$ , not only large exfoliation pits but also cluster-like oxide

particles (analyzed by EDS results in Table 3) are generated in the specimens when  $x=1$  and 2 (Fig. 8b<sub>2</sub> and 8c<sub>2</sub>), which originate from the oxidation of exfoliated substrate and the filling of the low-lying exfoliation pits during the wear process. Meanwhile, the appearance of cracks (Fig. 8c<sub>2</sub>) deteriorates the wear resistance. When  $x=3$ , the EDS result of wear track is shown in Fig. 9, and the Si and N elements are not found in the wear track, indicating that the wear mechanism of composite is not adhesive wear. A reduction in spalling pits and shallow wear traces is observed, which is probably related to the improvement of the wear resistance, considering the

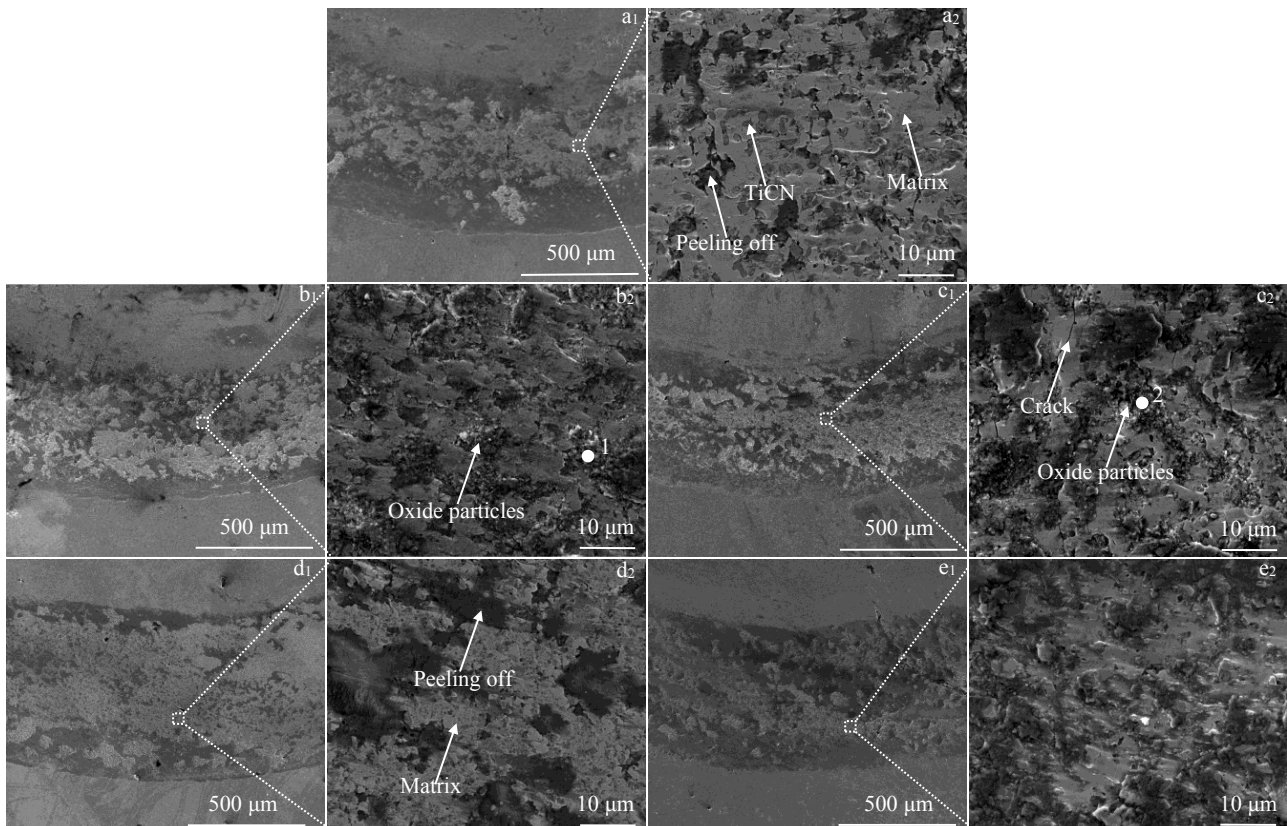


Fig.8 Wear morphologies (a<sub>1</sub>~e<sub>1</sub>) and detailed images (a<sub>2</sub>~e<sub>2</sub>) of Fe-Cr-xC/TiCN composites: (a<sub>1</sub>, a<sub>2</sub>)  $x=0$ , (b<sub>1</sub>, b<sub>2</sub>)  $x=1$ , (c<sub>1</sub>, c<sub>2</sub>)  $x=2$ , (d<sub>1</sub>, d<sub>2</sub>)  $x=3$ , and (e<sub>1</sub>, e<sub>2</sub>)  $x=4$

**Table 3** EDS results of points in Fig.8 (at%)

| Point | Fe    | Cr   | O     | Ti   |
|-------|-------|------|-------|------|
| 1     | 37.56 | 6.09 | 52.39 | 3.96 |
| 2     | 30.90 | 5.09 | 56.87 | 7.14 |

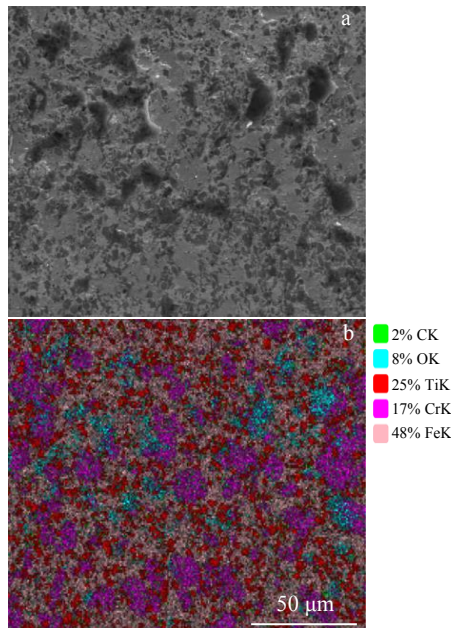


Fig.9 Image (a) and element distribution (b) of wear track of Fe-Cr-xC/TiCN composite with  $x=3$

significant decrease in the wear rate and the friction coefficient (Fig. 7). This behavior is mainly attributed to the wear-resistant skeleton which consists of carbides, such as  $(Cr, Fe)_7C_3$  and TiCN carbides, and the homogeneously distributed microstructures. During the wear process, plastic deformation occurs in the specimen. The poor plasticity causes the hard phase to peel off easily, while the  $(Cr, Fe)_7C_3$  carbides and TiCN particles are embedded in the matrix, and the matrix can play a role in resisting deformation and provide a good support to prevent the hard phase from spalling from the matrix. When  $x=4$ , the worn surface is rough and uneven due to the transfer layer formed by debris accumulation, leading to the high friction coefficient and wear rate.

### 3 Conclusions

1) The  $(Cr, Fe)_7C_3$  carbides form in Fe-Cr-C/TiCN composites by spark plasma sintering (SPS) process after addition of carbon black.

2) The relative density and hardness of composites are improved significantly with the increase of carbon black content, showing a maximum value of 99.7% and 12500 MPa, respectively.

3) When the carbon black content is 3wt% , a stable friction coefficient (0.320) and a small wear rate ( $6.8 \times 10^{-4}$

$\text{mm}^3 \cdot \text{N}^{-1} \cdot \text{m}^{-1}$ ) are achieved, and thus the composite exhibits an excellent wear resistance.

### References

- Chen M, Zhuang Q, Lin N et al. *Journal of Alloys and Compounds*[J], 2017, 701: 408
- Gómez B, Jiménez-Suarez A, Gordo E. *International Journal of Refractory Metals & Hard Materials*[J], 2009, 27(2): 360
- Gómez B, Gordo E, Torralba J M. *Materials Science and Engineering A*[J], 2006, 430(1-2): 59
- Ding H S, Liu S Q, Zhang H L et al. *Materials & Design*[J], 2016, 90: 958
- Umanskii A P. *Powder Metallurgy and Metal Ceramics*[J], 2001, 40(11): 637
- Dizaji V R, Rahmani M, Sani M F et al. *International Journal of Machine Tools and Manufacture*[J], 2007, 47(5): 768
- Li Y, Liu N, Zhang X et al. *International Journal of Refractory Metals & Hard Materials*[J], 2008, 26(1): 33
- Alvaredo P, Dios M, Ferrari B et al. *Journal of Alloys and Compounds*[J], 2019, 770: 17
- Mojisola T, Ramakokovhu M M, Raethel J et al. *Materials Today Communications*[J], 2019, 20: 100 606
- Alvaredo P, Gordo E, Van der Biest O et al. *Materials Science and Engineering A*[J], 2012, 538: 28
- Alvaredo P, Bruna P, Crespo D et al. *International Journal of Refractory Metals & Hard Materials*[J], 2018, 75: 78
- Alvaredo P, Tsipas S A, Gordo E. *International Journal of Refractory Metals & Hard Materials*[J], 2013, 36: 283
- Tang X H, Chung R, Pang C J et al. *Wear*[J], 2011, 271(9-10): 1426
- Huang Z, Ma S, Xing J et al. *International Journal of Refractory Metals & Hard Materials*[J], 2014, 45: 204
- Gu J H, Xiao P G, Song J Y et al. *Journal of Alloys and Compounds*[J], 2018, 740: 485
- Jiang J P, Li S B, Hu S J et al. *Materials Chemistry and Physics* [J], 2018, 214: 80
- Doğan Ö N, Hawk J A, Tylczak J H. *Wear*[J], 2001, 250(1-12): 462
- Xie G L, Sheng H, Han J T et al. *Materials & Design*[J], 2010, 31(6): 3062
- Du J, Chong X Y, Jiang Y H et al. *International Journal of Heat and Mass Transfer*[J], 2015, 89: 872
- Kan W H, Albino C, Dias-da-Costa D et al. *Materials Characterization*[J], 2018, 136: 196
- Zhang Z, Chen Y, Zhang Y et al. *Journal of Alloys and Compounds*[J], 2017, 704: 260
- Onuoha C C, Kipouros G J, Farhat Z N et al. *Journal of Alloys and Compounds*[J], 2019, 784: 519
- Zeng W, Yu D L, Ma Y L et al. *Materials Research Express*[J], 2019, 6(12): 126 514
- Luo Z C, Ning J P, Wang J et al. *Wear*[J], 2019, 432: 202 970

- 25 Khvan A V, Hallstedt B, Broeckmann C. *Calphad*[J], 2014, 46: 24
- 27 Bonny K, De Baets P, Vleugels J et al. *Wear*[J], 2009, 267(9-10): 1642
- 26 Alvaredo P, Mari D, Gordo E. *International Journal of Refractory Metals & Hard Materials*[J], 2013, 41: 115

## 碳黑含量对放电等离子烧结 Fe-Cr-C/TiCN 复合材料组织和耐磨性的影响

李学军, 刘颖, 叶金文, 周廷川, 陈道颖  
(四川大学材料科学与工程学院, 四川成都 610065)

**摘要:** 采用机械合金化和放电等离子烧结法制备了不同碳含量的 Fe-Cr-C/TiCN 复合材料。通过扫描电镜、X 射线衍射、维氏硬度和球-盘式摩擦试验, 系统地研究了碳含量对 Fe-Cr-C/TiCN 复合材料组织和磨损性能的影响。结果表明, 在含碳量为 1.0%~5.0% (质量分数, 下同) 的烧结样品中形成了  $(\text{Cr, Fe})_7\text{C}_3$  碳化物, 而当碳含量达到 4.0%~5.0% 时, 出现了  $(\text{Cr, Fe})_3\text{C}$  相。碳含量对 Fe-Cr-C/TiCN 复合材料的组织均匀性和致密化有着较为重要的影响, 当烧结温度为 ~1000 °C 时, 致密度由未加碳时的 95.0% 提高到的 99.7% (含碳量为 3.0%), 说明已实现了完全致密化。当含碳量为 3.0% 时, 维氏硬度达到 11 940 MPa。此外, 添加适量的碳 (3.0%) 有助于获得良好的磨损性能, 即摩擦系数波动范围小, 平均摩擦系数为 0.320, 磨损率为  $6.8 \times 10^{-4} \text{ mm}^3 \cdot \text{N}^{-1} \cdot \text{m}^{-1}$ 。

**关键词:** Fe-Cr-C/TiCN 复合材料; 碳; 放电等离子烧结; 显微组织和耐磨性

---

作者简介: 李学军, 男, 1994 年生, 硕士, 四川大学材料科学与工程学院, 四川成都 610065, 电话: 028-85405332, E-mail: 15198159377@163.com